Solid Freeform Fabrication 2018: Proceedings of the 29th Annual International Solid Freeform Fabrication Symposium – An Additive Manufacturing Conference
Reviewed Paper

Effect of energy density on the consolidation mechanism and microstructural evolution of laser cladded functionally-graded composite Ti-Al system

E. O. Olakanmi[1*], M. Sepako[1], J. Morake[1], S. Kutua[1], S. E. Hoosain[2], S. L. Pityana[2].

[1]Botswana International University of Science & Technology, Palapye, Botswana.

[2]Laser Enabled Manufacturing, NLC, Council for Scientific & Industrial Research, Pretoria. South Africa.

*Corresponding author: olakanmie@biust.ac.bw

Abstract: The engagement of additive manufacturing (AM) technology in developing intermetallic coatings involves additional heat treatment with a view to obtaining desirable microstructure and mechanical properties. This eventually increases the lead time and the manufacturing cost. To address these challenges, this study explores the fabrication of gradient and laminar structures of titanium aluminide (Ti-Al) composite coatings deposited on Ti-6Al-4V substrate via a single step laser cladding (LC). The alterations in microstructural properties, chemical composition and phase analysis of the coatings reinforced with TiC were investigated as a function of laser energy density. Evaluation of the deposited samples reveals that FGM composite clads were fabricated from Ti-Al blended with TiC when LED was set at 17.50 J/mm^2. At the selected LED, a thermo-positive reaction between the constituents' materials was induced and it resulted in the formation of intermetallic compounds (e.g. Ti_2AlC, γ and α_2 matrix phases) with a microhardness more than that of the substrate (Ti-6Al-4V alloy). This study provides new insights on the selection of process parameters for the coating manufacturers while employing low cost- and time-effective LC process for fabricating functional graded Ti-Al coatings.

Keywords: Functionally graded materials (FGM); Laser cladding (LC); Chemical composition; Titanium aluminide (Ti-Al).

1. INTRODUCTION:

Engineering components fabricated from functionally graded materials (FGM) are characterised with differing microstructural, mechanical and physical properties due to gradual alteration in chemical composition over its entire volume with a view to achieving superior service performance [1, 2]. FGMs ensure that its constituent dissimilar materials compensate for each other's demerits so as to manufacture a product with improved service performance relative to each of the parent materials when fabricated singly. Due to these reasons, FGMs are becoming increasingly popular in aerospace, nuclear, electronics, medical and chemical industries as seen in Nazarov and co-investigators [3] who demonstrated the potential of selective laser melting (SLM) fabricated functionally graded nickel aluminide (Ni-Al) system in manufacturing aviation components.

FGMs have been manufactured from Fe_3Al and SS316L [4]; Ti-6Al-4V and SS316 stainless [1]; nickel aluminide (Ni-Al) [3]; and titanium aluminide (Ti-Al) [5, 6] for various technological applications. Among various FGM systems, titanium aluminide (Ti-Al) are attracting increasing industrial and academic attention because of its superior elastic modulus, specific strength, creep strength and excellent temperature oxidation resistance [7, 8]. Nevertheless, Ti-Al structural parts are characterised with undesirable room temperature ductility, susceptibility to cracking and poor wear resistance [9-11]. Meanwhile, it has been established that controlled dispersion of reinforced particulates into FGM titanium aluminide matrix could enhance its wear resistance as well as associated microstructural and mechanical properties [9].

Among the manufacturing routes engaged in fabricating FGMs and its composites are selective laser melting (SLM) [3]; laser cladding (LC) [8, 9]; friction stir processing [12]; laser metal deposition [1, 4, 6] and self-propagating high temperature synthesis [5]. Of all these manufacturing routes, laser-based manufacturing (LbM) techniques such as LC imparts minimal heat-affected zone (HAZ) and dilution, reduced residual stress and improved metallurgical bonding when engaged in extending the service life of engineering components. Therefore, this study employs LC combined with pre-heating in depositing Ti-Al reinforced particulate FGM composite on Ti-6Al-4V substrate. The use of pre-heating in eliminating crack-susceptibility of engineering parts had been demonstrated in LbM.

Ti-6Al-4V is characterised with high strength and corrosion resistance, however, it's technological application in the automotive, aerospace, and power-generation industries is hindered by its limited operating temperature (400 ^oC) and poor wear resistance [13, 14]. This challenge can be overcome by incorporating reinforced particles into the FGM Ti-Al matrix in an attempt to increase the range of service temperature at which parts made in Ti-6Al-4V can be utilised as well as improve its wear resistance. Meanwhile, a search through the databases reveals that only a single study [9] had dwelt on LC fabricated FGM reinforced particulate composites till date. The study by Abboud and co-investigators [9] only considered the effects of scan velocity, powder feed rates and number of layers on the geometrical characteristics, microstructural variation and wear properties of Ti-Al/TiB_2 FGM composites. Findings from the study pointed out that the samples were porous and characterised with cracks. In order to establish a basis for manufacturing FGM parts for extending the high temperature service life and wear resistance of Ti-6Al-4V components in the automotive, aerospace, and power-generation industries, this study advances on the work of Abboud *et al.*, (1994) by considering the effects of laser energy density (LED) on the consolidation mechanism, microstructural evolution, microhardness, phase analysis and chemical composition of Ti-Al/TiC FGM composites fabricated with LC process combined with pre-heating. LED indicates the combined influence of laser power (P), scanning velocity (V) and beam diameter (d) in order to understand the role of thermal transfer in the solidification mechanism and microstructural development of Ti-Al/TiC FGM composite coatings.

2. MATERIALS AND METHODOLOGY:

2.1 Materials:

This study employed commercially available elemental gas atomised aluminium (Al: 45-90 µm), grade 1 titanium (Ti: 45-90 µm) and irregularly shaped titanium carbide (TiC: 45-90 µm) morphology. The purity of Ti, Al and TiC powders was 99.9%. The powders were supplied by TLS, Technik GmbH. The feed rate in g/min of each powder was determined via the flowability graphs. The component ratio of the FGM composite constituents was determined by using the ratio of the feed rate of the parent materials. Titanium aluminide (Ti-Al) system consisting of 50%wtTi-50wt%Al was formulated initially and the morphologies of the blended powders and that of TiC are shown in Figures 1a and b respectively. Figures 1c and d show the EDS analysis identifying the elemental composition of the blended 50%wtTi-50wt%Al and TiC powders respectively. Ti-Al was then blended with TiC in varying proportion as shown in Table 1 which depicts the gradual variation of composition across the volume of the FGM.

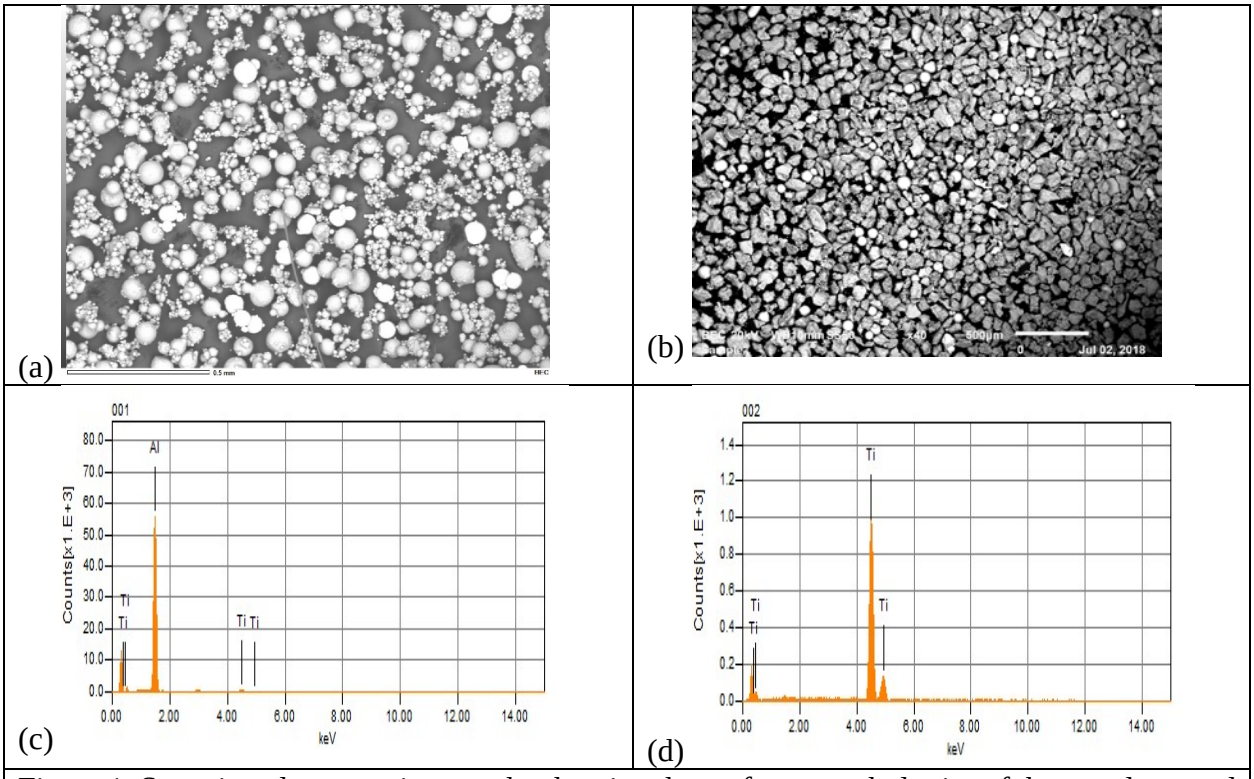

Figure 1: Scanning electron micrographs showing the surface morphologies of the powders used in this study (a) Titanium aluminide (Ti-Al); (b) Titanium carbide (TiC); and the EDS analysis confirming the elemental compositions of the powders (c) Titanium aluminide (Ti-Al); (d) Titanium carbide (TiC);

Table 1: Composition of powder blends used in fabricating each layer of the FGM composite clads.

No. of layer	Composition of powder blends for each layer
5	60% Ti-Al + 40wt% TiC
4	70% Ti-Al + 30wt% TiC
3	80% Ti-Al + 20wt% TiC
2	90% Ti-Al + 10wt% TiC
1	100% Ti-Al

2.2 Methodology

Prior to deposition of FGM composite materials, Ti-6Al-4V substrates with dimension 100 mm x 100 mm x 5 mm were cleaned with acetone in an attempt to remove impurities from its surface and enhance the quality of the laser clad. Table 2 shows the process parameters used in depositing the FGM reinforced particulate composite in this study. These parameters were adopted on the basis of a prior study carried out by Tlotleng *et al.,* [10] in which it was established that Ti-Al parts with desirable mechanical properties can be fabricated within the range of selected parameters. Laser energy density (LED) in J/mm^2 is defined as shown in (i)

$$LED = {}^{P}/_{V * d} \qquad (i)$$

Table 2: Process parameters used in depositing the FGM reinforced particulate composite.

Laser power (kW)	1.25, 1.50, 1.75
Scan speed (m/min)	1.50
Spot diameter (mm)	4.00
Energy density (J/mm^2)	12.50, 15.00, 17.50
Pre-heating temperature (^{o}C)	400.00
Standoff distance (mm)	12.00
Shielding gas flow rate (l/min)	10.00
Carrier gas flow rate (l/min)	2.00

The deposition of the FGM particulate reinforced composite in single track and multi-layers was achieved via a 3kW IPG continuous fiber laser system. In order to inject the FGM constituent materials into the melt pool on a substrate pre-heated at 400 ^{o}C, a 3-way coaxial nozzle system connected to a 5-axis CNC machine and a 1.5 bar GTV multi-hopper powder feed system was employed to serve this purpose. The powder feed system regulates the powder feed rate through its rotary speed. As reported earlier on, the flowability graphs of the powders were used in determining the component ratio of the FGM constituent materials as shown in Table 1. The shielding and carrier gases used in the experimental work are both made of argon gas with the specified flow rates in Table 2. Samples produced in each parameter shown in Table 2 were replicated twice. Since the deposition is continuous at the middle of the tracks, cross-sections of the deposited FGM clad samples were obtained at the middle of the track for microstructural and

compositional characterisation. Thereafter, the sectioned FGM clads were ground and polished to a 0.04 µm (OP-S suspension) surface finish with a Struers TegraForce-5 auto/manual polisher. The samples were etched in Keller's reagent for 2 to 3 minutes so that the microstructural characteristics were determined by Olympus optical microscope equipped with Analysis® software.

A scanning electron microscope (SEM), Jeol JSM-7100F equipped with energy dispersive X-ray spectroscopy (EDS) was used to carry out the microstructural and elemental analysis of the FGM composites. The SEM-EDS facility equipped with a video camera for observing the sample stage as its height is controlled used the NSS software for analysis. The phase composition of the FGM composite clads was identified via X-ray diffraction (Model Bruker D8 Advance.) with a Cu Kα monochromator radiation source. Material PDF files were used in identifying the phases present in the FGM composite coatings. Microhardness values of the FGM composite coatings were determined by using a Matsuzawa Seiko Vickers microhardness tester model MHT-1. The indenting load used was 500 g with a dwell time of 10 seconds used for each indentation. Microhardness measurements were taken along the length of the coating at 100 µm spacing as well as the interface between the substrate and the FGM composite coating. The experimental findings reported in this study were the average values of the corresponding results of the two groups of experiments.

3. RESULTS AND DISCUSSION:

3.1 Analysis of optical micrographs of FGM composite clads

Optical micrographs (OM) of the FGM composites revealing the developed microstructures at its lower, middle and upper sections (see Figures 2a-i) were examined with a view to understanding how variation in LED has altered the microstructure across its volume. Based on microstructural evidence obtained from Figure 2, irrespective of the amount of LED dissipated into the fabricating the FGM, the particle size of unmelted titanium carbide had diminished in varying degrees relative to the particle size of the starting powder which lies between 45 to 90 µm (Figure 1b). This suggests that TiC particles melted and dissolved in the melt pool. Furthermore, independent of the amount of LED employed during LC processing, it is also noted that the sizes of unmelted TiC particles in the FGM composite samples tend grow increasingly as follows: top layer → middle layer → bottom layer. This implies that increased consolidation occurred at the lower section in comparison to the top section of the FGM. In concurrence with Shishkovsky and co-investigators [6], the growth in the size of unmelted TiC particles as well as increased consolidation from the top layer to the lower layer of the FGM composite samples, irrespective of the LC process parameters, could be attributed to the phenomenon of directional solidification in which heat is dissipated away from the top layer to bottom layer.

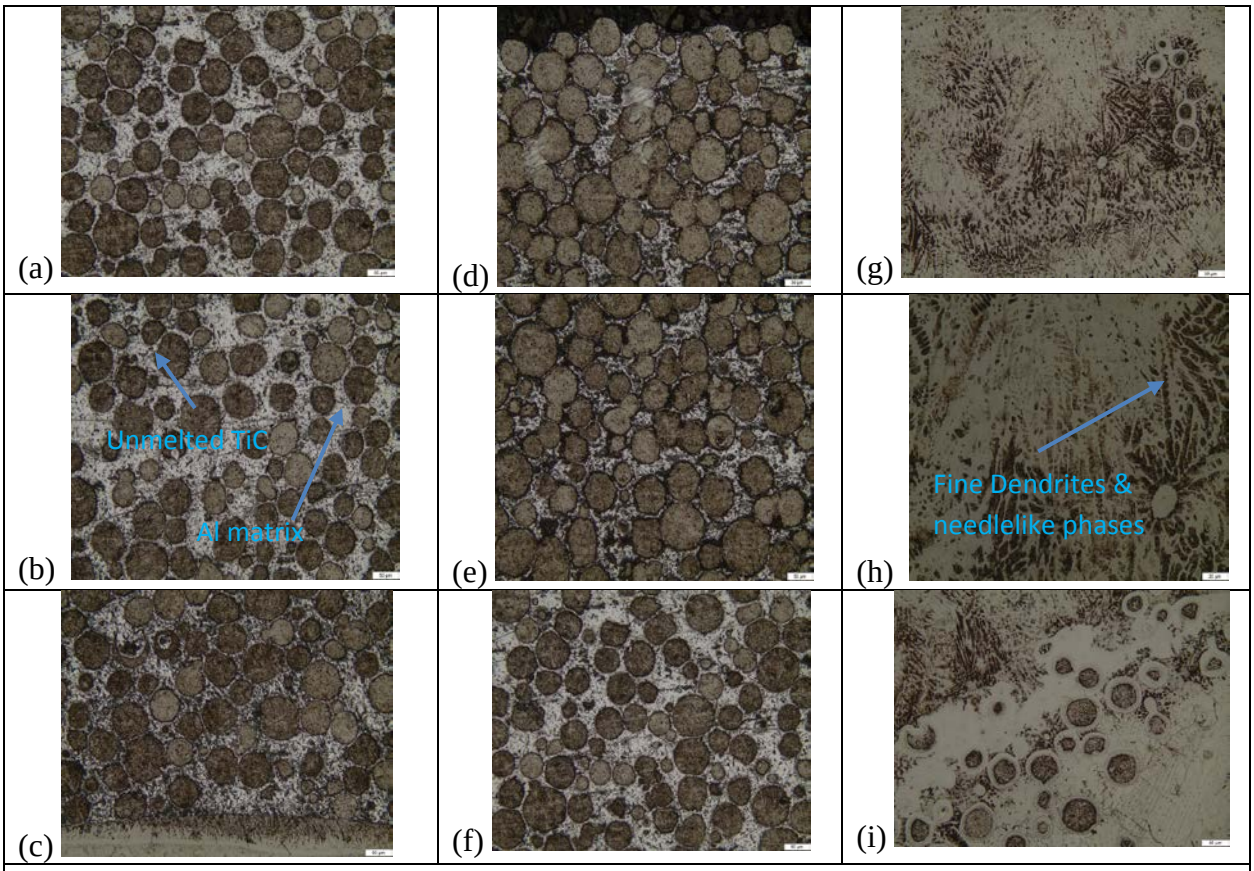

Figure 2: Optical micrographs of the FGM composite fabricated with 12.5 (a, b, c); 15.0 (d, e, f) and 17.5 J/mm^2 (g, h, i) viewed at the top layer(a, d, g); middle layer (b, e, g) and lower layer (c, f and i).

Figures 2a-c, d-f, and g-i show the optical micrograph images of the FGM composite fabricated with 12.50, 15.00 and 17.50 J/mm^2 respectively. These micrographs establish that the amount of TiC melting and dissolving in the melt pool varies as the LED dissipated during the LC processing of FGM samples. It is also evident from the micrographs that the sizes of unmelted TiC particles reduce as follows: 12.50 J/mm^2 → 15.00 J/mm^2 → 17.50 J/mm^2. The nature of microstructure evolving at the top, middle and bottom layers of FGM samples fabricated with LED of 17.5 J/mm^2 is presented in Figures 2g, h and i respectively. The sample made with LED of 17.50 J/mm^2 is distinguished from those fabricated with 12.50 J/mm^2 and 15.00 J/mm^2 as its microstructure is characterised with unmelted TiC particles as well as fine dendrite and needlelike phases at all location across the volume of the FGM. In addition, dendrites are finest at the top layer in comparison to the middle and lower layers.

3.2 Scanning electron micrographs and EDS analysis of FGM composite clads

Scanning electron micrographs (SEM) of the FGM composite samples fabricated with LED of 12.50, 15.00 and 17.50 J/mm^2 are shown in Figures 3a-c, d-f, and g-i respectively with a view to further highlighting on the distinguishing characteristics of each sample. It is evident from Figures 3a-c that that the microstructures of the FGM composite consists of grey-coloured

unmelted TiC particles (1), white-coloured ring region surrounding the unmelted TiC particle (2) and dark-coloured region (3). Comparative analysis of FGM composite samples fabricated with 12.50 J/mm^2 (Figure 3a-c) and 15.00 J/mm^2 (3d-f) reveals that the thickness of white-coloured ring regions are larger in the latter than the former. The thickness of these white-coloured ring region is also noted to be increasing from top to lower layers of the FGM samples irrespective of the selected process parameters. Meanwhile, the width of regions 1 and 3 have reduced in samples fabricated with 15.00 J/mm^2 (3d-f) relative to that of 12.50 J/mm^2.

EDS analysis was carried with a view to gaining insight into the chemical composition of the regions 1, 2 and 3 formed in FGM samples fabricated with 12.50 J/mm^2 and 15.0 J/mm^2. EDS findings reported in Table 3 confirm that the grey-coloured region 1 is rich in titanium with trace quantity of carbon; the white-coloured ring region 2 consists of aluminium, carbon and titanium; while the dark coloured region 3 consists of aluminium and carbon with trace quantity of titanium. The formation of white-coloured ring region 2 indicates the occurrence of metallurgical reaction between aluminium, titanium and carbon while the existence of region 3 indicates there was diffusion of carbon to aluminium rich dark areas.

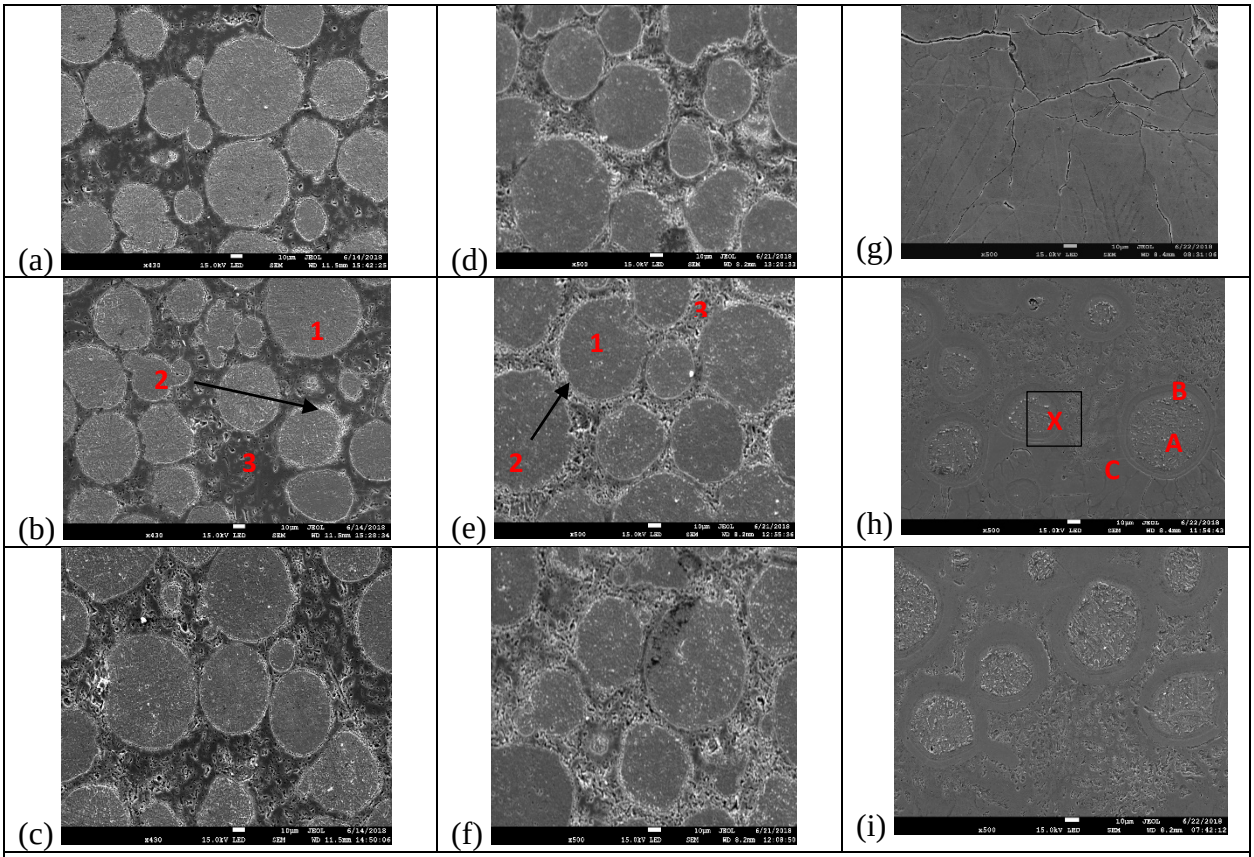

Figure 3: Scanning electron micrographs (SEM) of the FGM composite fabricated with 12.5 (a, b, c); 15.0 (d, e, f) and 17.5 J/mm^2 (g, h, i) viewed at the top layer (a, d, g); middle layer (b, e, g) and lower layer (c, f and i).

Table 3: Typical chemical composition of FGM samples fabricated with LED of 12.0 J/mm^2 and 15.0 J/mm^2.

	C	Al	Ti
1	0.87		99.13
2	8.33	85.68	5.98
3	5.17	94.19	0.64

Analysis of Figures 3g-i reveal the evolution of distinct microstructural features for FGM composite samples fabricated with 17.5 J/mm^2. For instance, three regions consisting of the core (A) surrounded by layers (B) and sandwiched between region C are shown in Figure 3h. The area marked X in Figure 3h is a representative area consisting of A, B and C which is observed at higher magnification (Figure 4). Figure 4 reveals that the core region 1 is surrounded by layers 2, 3 and 4 with the layers sandwiched in lighter grey region 5. The EDS analysis of the regions is shown in Table 4.

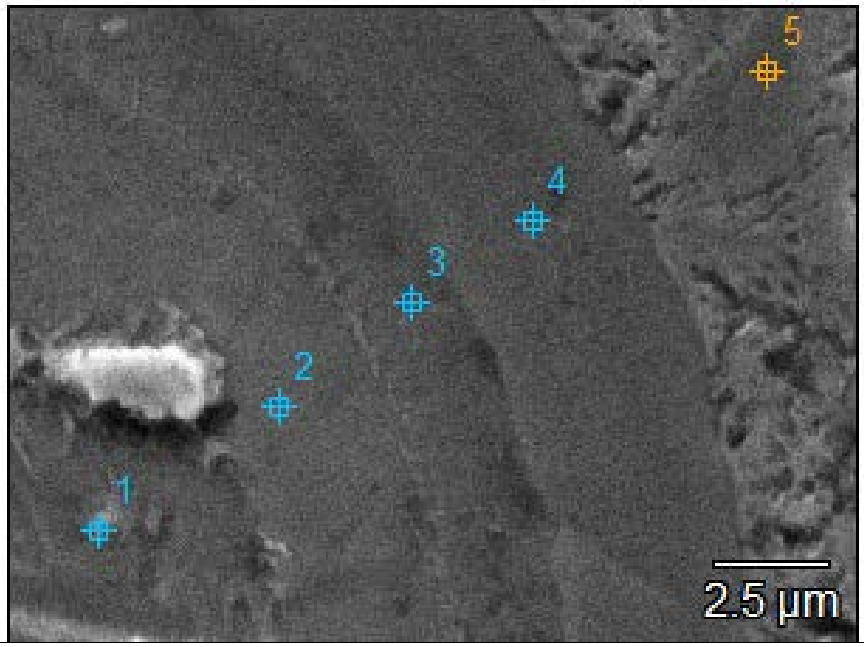

Figure 4: SEM observation of regions A, B and C at higher magnification

Table 4: Typical chemical composition of regions A, B and C.

	C	Al	Ti
1	0.80		99.20
2	0.92	0.97	98.11
3	1.74	11.65	86.60
4	2.12	20.88	77.00
5	2.60	37.56	59.84

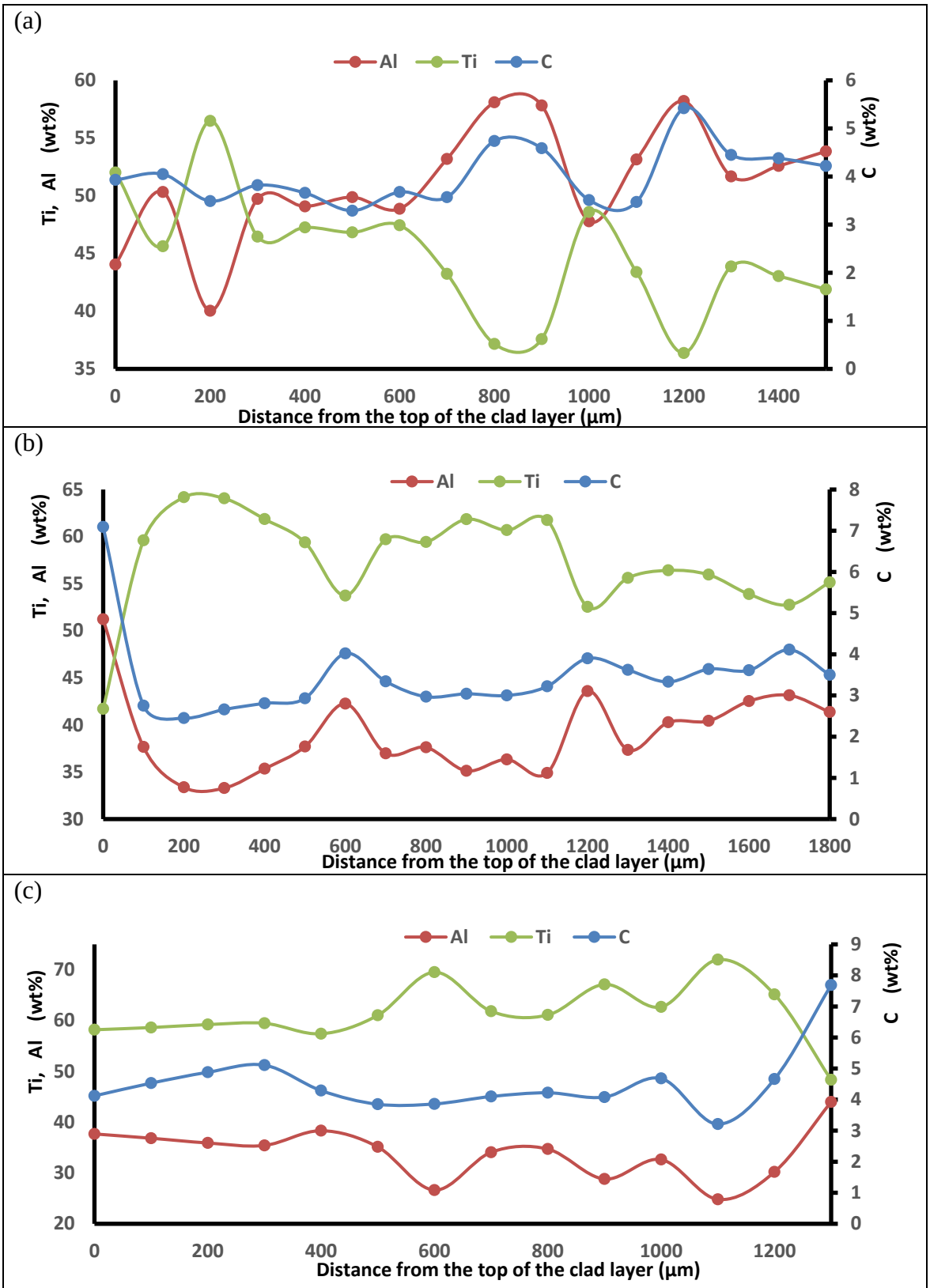

Figure 5: EDS point test data for the composition curves of FGM composite fabricated with (a) 12.50 J/mm^2 (b) 15.00 J/mm^2 and (c) 17.50 J/mm^2

Analysis of Figure 4 and Table 4 confirm that an in-situ reaction synthesis occurred between Ti-Al and TiC powders when LED of 17.5 J/mm^2 was dissipated for processing as isolated titanium rich (1) and aluminium rich (3) regions which are associated with FGM composites fabricated with lower LED (Figures 3a-c; d-f) have depleted in size (Figures 3g-i). This occurred as aluminium and carbon atoms diffused inward into the titanium core.

Figures 5a, b and c depict the EDS point test data for the composition curves of FGM composite fabricated with 12.50, 15.00 and 17.50 J/mm^2 respectively. An observation of Figure 5 shows that the EDS of all FGM composite clads possess the following features in common: immediate lift and dip, as well as up and down stagger irrespective of the laser energy density employed during fabrication. Meanwhile, intersection is only evident across the length of the sample fabricated with 12.50 J/mm^2 (Figure 5a) and at the top layer of the FGM composite clad deposited with 15.00 J/mm^2 (Figure 5b). The occurrence of these features on the compositional curves suggests the trends in the elemental concentration across the volume of the FGM composite. It is evident from Figures 5a, b and c that at instances when titanium diffuses faster, both aluminium and carbon tend to diffuse very slowly and vice-versa. At 12.50 J/mm^2, it is established that Ti atoms diffuse slower than aluminium and carbon atoms (Figure 5a). As the LED increases to 15.00 J/mm^2 and 17.50 J/mm^2, titanium atoms diffuse faster than aluminium and carbon atoms (Figures 5b and c). With LED set at 12.50 J/mm^2, the concentration of diffused aluminium atoms are above the expected values of 50wt%, 45wt%, 40wt%, 35wt% and 30wt% for each of the 1st, 2nd, 3rd, 4th and 5th layers respectively whereas the concentration of dissolved titanium atoms across at all the layers are below the expected values. This could be attributed to the fact that the dissipated LED is only effective at melting much of aluminium atoms to the detriment of titanium atoms. Meanwhile, at LED of 15.00 J/mm^2 and 17.50 J/mm^2, the concentration of aluminium atoms are much well below the expected values across the layers while those of titanium are well above the expected concentration values across the layers. It is pertinent to note that the concentration of dissolved titanium atoms across the layers of the FGM composite clad fabricated with 17.50 J/mm^2 are higher than those of 15.00 J/mm^2 while the converse is true for aluminium. The concentration of diffused carbon atoms across layers is constant at values varying between 3.00 to 4.00 wt% for samples fabricated with 15.00 J/mm^2 and 17.50 J/mm^2. The concentration of diffused carbon atoms across FGM layers at 15.00 J/mm^2 and 17.50 J/mm^2 is lower than that of 12.50 J/mm^2. Reduced concentration of aluminium below the expected values across the layers at 15.00 J/mm^2 and 17.50 J/mm^2 indicate that aluminium atoms might have evaporated as the specified LED might have induced processing temperature higher than the melting point of aluminium. Increased concentration of titanium atoms for samples deposited with 15.00 J/mm^2 and 17.50 J/mm^2 suggests increasing trend in the formation of intermetallic compounds between Ti, Al and C atoms. Meanwhile, it is anticipated that the phase composition of intermetallic compounds forming from metallurgical reactions between Ti, Al and C atoms will increase in the following order: 12.50 J/mm^2 → 15.00 J/mm^2 → 17.50 J/mm^2.

3.3 XRD analysis of FGM composite clads

XRD analysis (Figure 6 and Table 5) of the samples confirms the formation of Ti_2AlC (titanium aluminide carbide) in the FGM composites in addition to γ and α_2 matrix phases while some TiC phases are still retained within the microstructure. The relative intensity of diffractive peaks (Figure 6) for α_2 in the FGM composite clads is significantly enhanced as LED increases. This emphasizes that increase in the volume fraction of α_2 matrix occurs as LED increases. Findings reported for Figures 3 and 5 as well as Tables 3 and 4 support this claim that the propensity of metallurgical reactions involving Ti and Al tends to increase as LED increases. According to Liu & DuPont [15], for a melt pool containing $>$ 2 at. pct. carbon at processing temperatures $>$ 2200 ^{o}C, primary TiC_{1-x} solidifies initially. Thereafter, a peritectic reaction in which TiC_{1-x} + L $\rightarrow$ Ti_2AlC occurs as the melt pool cools down to 2200 ^{o}C. Further cooling of the melt pool below 2200 ^{o}C leads to the precipitation of the ternary Ti_2AlC because of depletion of carbon content in the liquid composition. Later, a different peritectic reaction in which L + Ti_2AlC $\rightarrow$ β-Ti(Al) occurs. Liu & DuPont [15] also reported that the reaction L + β $\rightarrow$ α + Ti_2AlC could occur at the final stage of LC processing. Given the available information from the work of Liu & DuPont [15], the phase transformation scheme for the FGM composite clads is elucidated as follows:

L $\rightarrow$ TiC + L $\rightarrow$ TiC + Ti_2AlC + L $\rightarrow$ TiC + Ti_2AlC + β + L $\rightarrow$ TiC + Ti_2AlC + α $\rightarrow$ TiC + Ti_2AlC + γ (TiAl) + α_2(Ti_3Al).

In agreement with Pedrix and co-investigators [16], increment in volume fraction of α_2 in the FGM composite clads with increased LED as seen in the XRD analysis suggests that increased carbon in solid solution as LED increases leads to enhancement in the stability of elevated temperature α phase. Furthermore, the Ti-Al-C phase diagram also confirms that the solubility of carbon in the α_2 phase is higher relative to that of γ phase [15]. Increased metallurgical reaction between Ti, Al and C at the highest LED adopted in this study (see Table 2) suggests that increased laser power enhances available heat being dissipated to the powder blends. Consequently, this raises the temperature of the melt pool as well as the propensity of the laser-material interaction to form an intermetallic compound as increasing amount of TiC dissolved into the melt pool. The precipitation of primary TiC from the melt upon solidification in all the samples could be attributed to the fact that the carbon content in the melt pool (Tables 3 and 4) is higher than 2 at. pct. irrespective of the LED adopted in fabricating the FGM composite clads. Although, the dissolved carbon content in the melt pool varies depending on the LED adopted for processing.

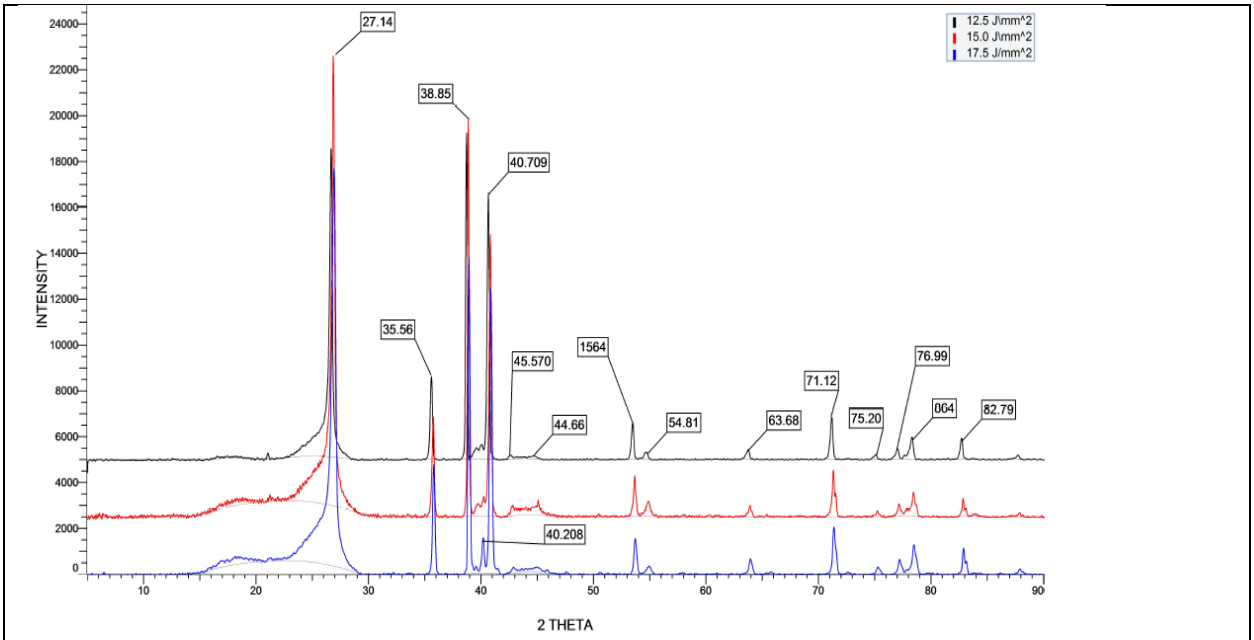

Figure 6: XRD analysis of FGM composite clad samples fabricated with LED of 12.50, 15.00 and 17.50 J/mm^2.

Table 5: XRD analysis showing the phases presented in FGM composite samples fabricated with varying LED.

Phase	2 Theta Angles	Phase Composition		
		12.50 J/mm^2	15.00 J/mm^2	17.50 J/mm^2
A: γ-TiAl	21.92,38.95,44.73,78.57	√	√	√
B: α_2-Ti_3Al	35.65, 40.90,53.81 64.64, 77.96	√	√	√
C: TiC	35.65, 40.90, 53.81, 76.92	√	√	√
D: Ti_2AlC	40.91,53.91	√	√	√
E: Ti	35.75,36,06,40,50,53,60,55,46,71,25			√

Each of the FGM composite clads fabricated in this study consists of different five layers regarding the composition and structure of each layer. Therefore, the composition and microstructure of each layer is a function of the composition of the powder blends as well as the LED. The dilution resulting from the melting of one layer upon the other as well as its solidification phenomenon is manipulated by the LED. It is expected that a minimum dilution between the first layer and the substrate is attained by selecting the appropriate LED parameter to impart the desirable composition. Further studies will explore the alteration in the composition across the five layers of the FGM composite clads with reference to the Ti-Al-C ternary system.

3.4 Microhardness of FGM composite clads

Figure 7 shows the microhardness ($HV_{0.5}$) across the layers of FGM composite clad samples at varying LED from the top surface of the deposits to the substrate. It is clear from Figure 7a that the microhardness across the layers was constant ($\sim$ 100 $HV_{0.5}$) and significantly less than that of the substrate. This outcome is not surprising as the applied LED of 12.50 J/mm^2 is not effective to initiate metallurgical reactions between Ti, Al and C to ensure formation of intermetallics which could have imparted higher microhardness across the FGM layers. A marginal increase in microhardness across the FGM layers is noted for samples deposited with LED of 15.00 J/mm^2 relative to that of 12.50 J/mm^2. The microhardness across the layers is however less than that of the substrate. In similarity to that of the sample deposited with 12.50 J/mm^2, there is no difference in the microhardness across the second to fifth layers except in the first layer in which the microhardness is $\sim$ 200 $HV_{0.5}$. This indicates that the adopted process parameter is just sufficient to initiate gradient composition in the first layer alone. With LED increasing to 17.50 J/mm^2, the microhardness profile (Figure 7c) obtained across the FGM composite clad layers is like that reported for two-layer functionally gradient Ti-Al/TiB_2 composite [9]. Except for the first layer, the microhardness across the last four layers is either equal to or higher than that of the substrate (Figure 7c). The impartation of microhardness values higher than that of the substrate at the last four layers of this sample points to (i) the Ti-Al matrix alloying with aluminium as well as the partial melting of TiC which results in the precipitation of primary TiC crystals; and (ii) refinement of the microstructure at these layers upon the occurrence of the phenomenon of rapid solidification. Meanwhile, reduced microhardness reported for the sample at the first layer and the interface could be attributed to the undesirable influence of the directional solidification in which excessive heat being transferred from the top layers to the first layers and the interface might have induced microstructural defects at the first layer and the interface.

Evidence from microstructural/microhardness studies, chemical composition and phase analysis of the samples indicates that reaction synthesis will not take place between Ti and Al when LED is less than 17.50 J/mm^2. Therefore, the formation of intermetallic compounds (e.g. Ti_2AlC, γ and α_2 matrix phases) results from thermo-positive reactions between Ti-Al. Prior to the commencement of the reaction synthesis via LC processing, the powder blends were heated near or thereabout the melting of aluminium. Consequently, molten aluminium reacts with Ti particles via a thermo-positive reaction which produces a range of products including the following: $3Ti + Al \rightarrow Ti_3Al$; $Ti + Al \rightarrow TiAl$. As a result, the temperature of the whole system is deemed to rise abruptly and this induces a chain of reaction in the entire system. With increasing LED raising the temperature of the system to the melting point of Ti or above, this initiates a violently thermo-positive reaction which produces molten Ti_2AlC (titanium aluminide carbide).

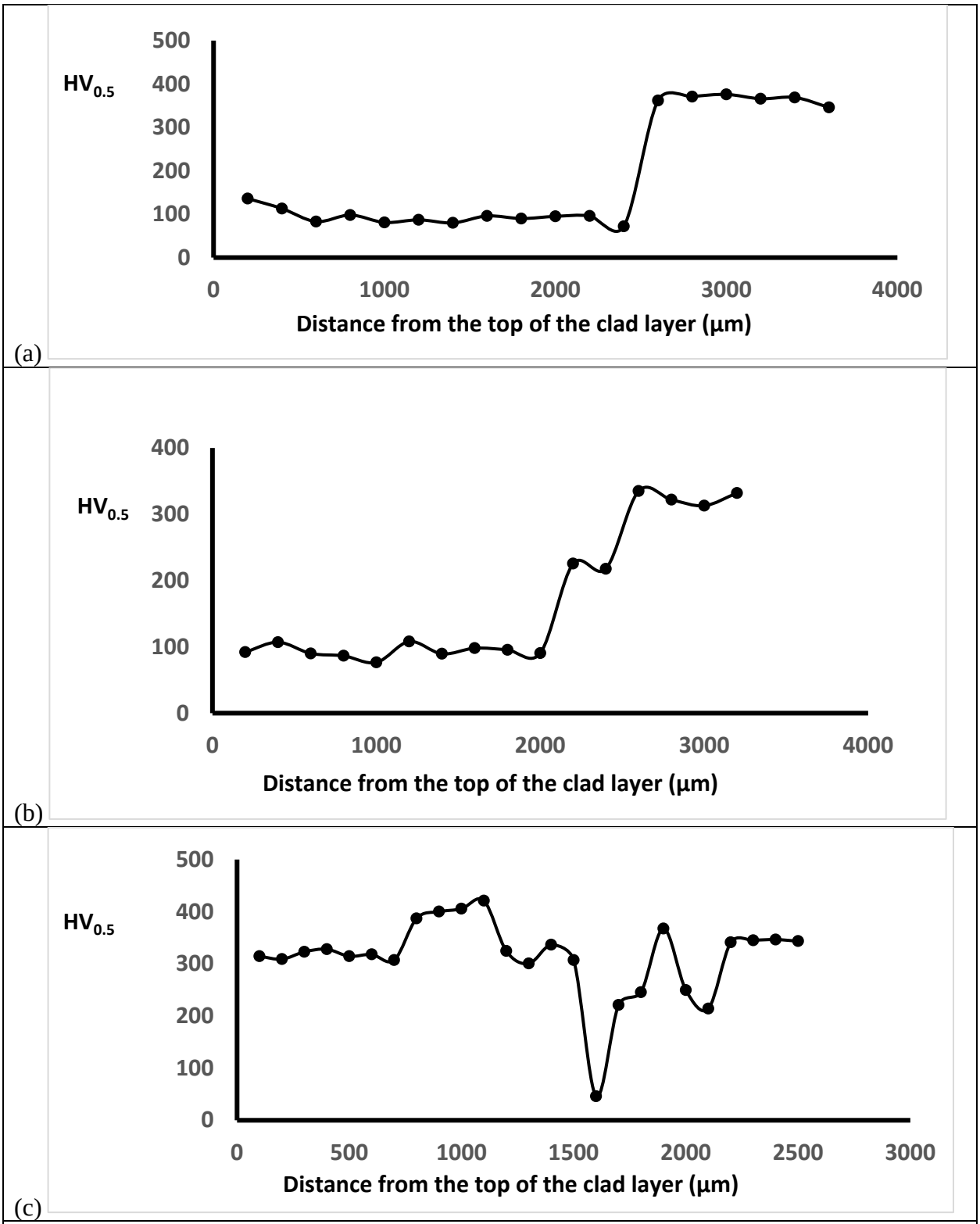

Figure 7: Microhardness ($HV_{0.5}$) across the layers of FGM composite clad samples at varying LED from the top surface of the deposits to the substrate (a) 12.50 J/mm^2., (b) 15.00 J/mm^2. and (c) 17.50 J/mm^2.

4. Conclusions:

1. Based on microstructural evidence obtained from this study, the particle size of unmelted titanium carbide diminished in varying degrees, depending on the applied LED, relative to the particle size of the starting powder which lies between 45 to 90 µm. This suggests that TiC particles melted and dissolved in the melt pool.

2. During the LC processing of the FGM composite clads, it was discovered that when titanium diffuses faster, both aluminium and carbon tend to diffuse very slowly and vice-versa. Moreover, titanium diffuses faster than both aluminium and carbon at higher LED.

3. When the LED was set at 12.50 J/mm^2 and 15.00 J/mm^2, the induced processing temperature associated with the synthesis reaction of the powder blends was just adequate to affect the melting of aluminium.

4. FGM composite clads were fabricated from Ti-Al blended with TiC when LED was set at 17.50 J/mm^2. At the selected LED, a thermo-positive reaction between the constituents' materials was induced and it resulted in the formation of intermetallic compounds (e.g. Ti_2AlC, γ and α_2 matrix phases).

5. The impartation of microhardness values higher than that of the substrate for the FGM composite clad fabricated with 17.50 J/mm^2 could be attributed to (i) the Ti-Al matrix alloying with aluminium as well as the partial melting of TiC which results in the precipitation of primary TiC crystals; and (ii) refinement of the microstructure at these layers upon the occurrence of the phenomenon of rapid solidification.

6. The composition and microstructure of each layer of the FGM composite is not only a function of the composition of the powder blends but also that of the LED.

REFERENCES:

L. Thijs, K. Kempen, J. P. Kruth et al.,"Fine-structured aluminium products with controllable texture by selective laser melting of pre-alloyed AlSi10Mg powder," Acta Materialia, 61(5), 1809-1819 (2013).

[1]
W. Li, S. Karnati, C. Kriewall, F. Liou, J. Newkirk, K.M.B. Taminger, W.J. Seufzer, Fabrication and characterization of a functionally graded material from Ti-6Al-4 V to SS316 by laser metal deposition," Additive. Manufacturing, 14, 95-104, (2017).

[2] Y. Zhang, W. Ni, Y. Li, "Effect of siliconizing temperature on microstructure and phase constitution of Mo–MoSi2 functionally graded materials," Ceramics International, 44, 11166-11171, (2018).

[3] A. Nazarov, V. A. Safronov, R. S. Khmrov, I. Shishkovsky, ”Fabrication of gradient structures in the Ni-Al system via SLM process,” Procedia IUTAM, 23, 161-166, (2017).

[4] T. Durejko, M. Ziętala, W. Polkowski, T. Czujko, “Thin wall tubes with Fe3Al/SS316L graded structure obtained by using laser engineered net shaping technology,” Materials & Design, 63, 766-774, (2014).

[5] C. Farley, T. Turnbull, M. L. Pantoya, E. M. Hunt, “Self-propagating high-temperature synthesis of nanostructured titanium aluminide alloys with varying porosity,” Acta Materialia, 59. 2447-2454, (2011).

[6] I. Shishkovsky, F. Missemer, I. Smurov, “Metal matrix composite with ternary intermetallic inclusions fabricated by laser direct energy deposition,” Composite Structures, 83, 663-670, (2018).

[7] S. E. Hoosain, S. L. Pityana, M. Tlotleng, T. Legopeng, “A comparative study on laser processing of commercially available titanium aluminide (TI-48AL-2CR-2NB) and in-situ alloying of titanium aluminide,” Presented at the 18th Annual International Rapid Product Development Association of South Africa (RAPDASA), 7-10 November 2017, Durban ICC, South Africa.

[8] B. N. Masina, T. Lengopeng, S. L. Pityana, M. Tlotleng, “Microstructure and Mechanical characterisation of TiAl coated on Ti64,” South African Journal of Industrial Engineering, 28, 172-177, (2017).

[9] J. H. Abboud, D. R. F. West, R. D. Rawlings, “Functionally gradient titanium-aluminide composites produced by laser cladding,” Journal of Materials Science, 29, 3393-3398, (1994).

[10] M. Tlotleng, T. Lengopeng, S. L. Pityana,. Evaluation of the microstructure and microhardness of laser-fabricated titanium aluminate coatings. Presented at the AMI Ferrous and Base Metals Development Network Conference 2016, 19-21 October 2016, Southern Sun Elangeni Maharani, Kwazulu-Natal.

[11] N. Mizuta, K. Matsuura, S. Kirihara, Y. Miyamoto, “Titanium aluminide coating on titanium surface using three-dimensional micro-welder,” Materials Science & Engineering A, 492, 199-204, (2008).

[12] M. Salehi, H. Farnoush, J. A. Mohandesi, “Fabrication and characterisation of functionally graded Al-Sic nano-composite by using a novel multi-step friction stir processing,” Materials & Design, 63, 419-426, (2014).

[13] N. Poondla, T. S. Srivastan, A. Patnaik, M. Petraroli, M. “A study of the microstructure and hardness of two titanium alloys: Commercially pure and Ti-6Al-4V,” Journal of Alloys & Compounds, 486, 162- 167, (2009).

[14] B. Cárcel, A. Serrano, J. Zambrano, V. Amigó, A. C. Cárcel, “Laser cladding of TiAl intermetallic alloy on Ti6Al4V: Process optimization and properties,” Physics Procedia, 56, 284-293, (2014).

[15] W. Liu, J. N. DuPoint, “Fabrication of carbide-particle-reinforced titanium aluminide-matrix composites by laser-engineered net shaping,” Metallurgical & Materials Transactions A, 35A, 1133-1140, (2004).

[16] F. Perdrix, M. Trichet, J. Bonnentien, M. Cornet, J. Bigot, “Relationships between interstitial content, microstructure and mechanical properties in fully lamellar Ti–48Al alloys, with special reference to carbon” Intermetallics, 9, 807-815, (2001).